Dynamical tuning of the chemical potential to achieve a target particle number in grand canonical Monte Carlo simulations

Cole Miles, Benjamin Cohen-Stead, Owen Bradley, Steven Johnston, Richard Scalettar, and Kipton Barros

Phys. Rev. E **105**, 045311 — Published 18 April 2022

DOI: 10.1103/PhysRevE.105.045311

Dynamical tuning of the chemical potential to achieve a target particle number in grand canonical Monte Carlo simulations

Cole Miles,[1,*] Benjamin Cohen-Stead,[2] Owen Bradley,[2] Steven Johnston,[3,4] Richard Scalettar,[2] and Kipton Barros[5,†]

[1] *Department of Physics, Cornell University, Ithaca, New York 14850, USA*
[2] *Department of Physics, University of California, Davis, California 95616, USA*
[3] *Department of Physics and Astronomy, The University of Tennessee, Knoxville, Tennessee 37996, USA*
[4] *Institute for Advanced Materials and Manufacturing, University of Tennessee, Knoxville, Tennessee 37996, USA*
[5] *Theoretical Division and CNLS, Los Alamos National Laboratory, Los Alamos, New Mexico 87545, USA*

We present a method to facilitate Monte Carlo simulations in the grand canonical ensemble given a target mean particle number. The method imposes a fictitious dynamics on the chemical potential, to be run concurrently with the Monte Carlo sampling of the physical system. Corrections to the chemical potential are made according to time-averaged estimates of the mean and variance of the particle number, with the latter being proportional to thermodynamic compressibility. We perform a variety of tests, and in all cases find rapid convergence of the chemical potential—inexactness of the tuning algorithm contributes only a minor part of the total measurement error for realistic simulations.

I. INTRODUCTION

A fundamental attribute of statistical mechanics is the equivalence of thermodynamic ensembles in the limit of large system size. In particular, the *canonical* ensemble, with fixed particle number, should be equivalent to a *grand* canonical ensemble in which the chemical potential μ is suitably selected to fix the average particle number. However, there may be practical reasons to prefer working in the grand canonical ensemble, particularly in the context of Monte Carlo (MC) simulations. In classical MC simulations, for example, moves that modify the particle number can be useful for reducing decorrelation times or for studying coexistence between phases [1–5]. Similarly, the starting point of many [6–12] (but not all [13–16]) finite temperature quantum Monte Carlo (QMC) simulations is the grand canonical partition function $Z = \mathrm{Tr}\,\exp[-\beta(H + \mu N)]$, where β is the inverse temperature, H is the Hamiltonian, and N is the number operator. The trace above runs over *all* quantum wavefunctions, not just those constrained to a fixed particle number.

In MC and QMC simulations, we often wish to specify the average particle number $\langle N\rangle$ directly, e.g., to fix the electron filling fraction. Determining the μ value which satisfies this condition has traditionally required a tedious manual search, with additional searches necessary after every update to the model parameters. Here we present a method to efficiently converge the chemical potential μ to a solution value that produces the desired mean particle number within the same MC/QMC simulation where measurements are performed. We take the chemical potential μ_t to be continually evolving in sampling time t. Corrections to μ_t are performed whenever new measurements N_t of $\langle N\rangle$ are collected.

A central challenge is that, in certain cases, it can be difficult to collect good statistical samples for systems with long autocorrelation times. That is, modifications to μ_t may not fully impact the samples N_t until quite some time later. We address this problem by employing increasingly long-time averages, which incorporate a fixed fraction of *the entire history of MC data.*

Roughly speaking, our proposed strategy for tuning μ_t is as follows: Given continually improving approximate measurements of the particle number $\langle N\rangle$ and compressibility $\kappa = \mathrm{d}\langle N\rangle/\mathrm{d}\mu$, we update the value of the chemical potential under the assumption of linear response. Our method shares some conceptual similarities with proportional–integral–derivative (PID) controllers, which have previously been applied to μ-tuning [17, 18]. A disadvantage of PID controllers is that they introduce several parameters that must be carefully selected for each new problem. In contrast, the method we introduce here is simple and works robustly across a wide range of problems using a single default set of algorithm parameters.

We benchmark the new method on two problems: (1) Tuning the applied field in the classical two-dimensional ferromagnetic Ising model to achieve a target magnetization, and (2) tuning the chemical potential in simulations of the quantum Holstein model to achieve a target electron filling fraction. For the Ising model, simulation temperatures approaching T_c give rise to long autocorrelation times, which can make it difficult to achieve good statistical sampling. For QMC simulations of the Holstein model, phonons mediate an effective attractive electron-electron interaction, which, in turn, gives rise to challenging metastability effects.

The benchmarks indicate that accurate measurements of a system with a specified mean particle number can be acquired from a *single* MC simulation run, with μ-tuning enabled throughout. This works because μ_t mostly converges within the burn-in period of the MC simulation. After burn-in there remains a small (and steadily decreasing) error in μ_t, but it does not seem to contribute

* cmm572@cornell.edu
† kbarros@lanl.gov

significantly to the overall statistical error in measurements.

II. METHOD

We present a method to tune any thermodynamic field according to its conjugate observable. For concreteness, consider the task of tuning the chemical potential μ to produce a target mean particle number, $\langle N\rangle = N^*$. The same method could be applied to a magnetic system, in which case one would replace μ with the applied magnetic field and $\langle N\rangle$ with the total magnetization (an example is considered in Sec. III A).

At fixed μ, one can estimate the mean particle number $\langle N\rangle$ using MC sampling. The compressibility κ will play an essential role in our tuning scheme. A fundamental result from thermodynamics states

$$\kappa = \frac{\mathrm{d}\langle N\rangle}{\mathrm{d}\mu} = \beta\,\mathrm{Var}[N], \tag{1}$$

where $\mathrm{Var}[N] = \langle N^2\rangle - \langle N\rangle^2$. Thus, κ can be estimated using the observed variance of N.

A. Prior work with iterated simulation

Previous work proposed the following μ-tuning strategy [17]: At fixed μ, run MC over some time window to collect statistical estimates $\overline{N}$ and $\overline{\kappa}$ of the mean particle number and compressibility. To find the chemical potential that will approximately achieve a target particle number N^*, solve for the μ' value that satisfies $\overline{\kappa} = (N^* - \overline{N})/(\mu' - \mu)$. Assign $\mu \leftarrow \mu'$ and repeat.

A practical challenge with this iterated update scheme is that it may be difficult to acquire sufficiently good estimates $\overline{N}$ and $\overline{\kappa}$. It is hard to know *a priori* how much sampling time should be devoted to any particular μ value. Statistical estimates of κ, associated with fluctuations in N, are particularly error prone. Also, if many iterative updates to μ are required, it would seem advantageous to incorporate information from *all* previous MC runs, not just from the most recent sampling window.

B. Dynamical μ-tuning

In contrast to the iterated simulation scheme, here we explore an approach where μ_t evolves dynamically in the context of a single simulation. At each iteration t, a MC update step or sweep is performed using the instantaneous value μ_t of the chemical potential. Next, the chemical potential is updated using the rule

$$\mu_{t+1} = \overline{\mu}_t + (N^* - \overline{N}_t)/\overline{\kappa}_t. \tag{2}$$

We use the notation $\overline{(\cdot)}_t$ to signify an appropriate time average over a subset of the sampled data up to time t. Note that *the effective window size is continually increasing with sampling time.* Many types of time-averaging are possible; for simplicity, we average over the most recent half of all collected data, weighting each sample equally. Averages of μ and N up to time t are defined as

$$\overline{\mu}_t = \frac{1}{L_t}\sum_{t'=\lceil t/2\rceil}^{t} \mu_{t'} \tag{3}$$

$$\overline{N}_t = \frac{1}{L_t}\sum_{t'=\lceil t/2\rceil}^{t} N_{t'}. \tag{4}$$

The ceiling function $\lceil\cdot\rceil$ rounds up to the nearest integer and $L_t \equiv t - \lceil t/2\rceil + 1$ is the number of samples in the average. We select this form for the running-time averages partly for simplicity, and partly because it allows updates in constant time, as described in Appendix A.

An important aspect of Eq. (2) is that it defines μ_{t+1} as a correction to the time-averaged chemical potential $\overline{\mu}_t$, and *not* as a correction to the previous instantaneous chemical potential μ_t. In this way, the estimator μ_t captures important information from the entire sampling history, and evolves on the same time scale as $\overline{N}_t$.

1. *Estimating compressibility*

The success of Eq. (2) depends crucially on the definition of the time-averaged compressibility $\overline{\kappa}_t$. Equation (1) suggests that we can estimate κ using the time-averaged variance,

$$\kappa_t^{\mathrm{fluc}} = \beta\,\overline{\mathrm{Var}}_t[N]. \tag{5}$$

For classical systems, $\overline{\mathrm{Var}}_t[N]$ is defined as the sample variance for the data $\{N_{t/2}, \ldots N_t\}$. For quantum systems, a slightly modified definition is given in Eq. (17). Generally, the fluctuation-based estimator κ_t^{fluc} becomes valid at late times, once μ_t settles to a near constant value. At early times, however, μ_t is evolving rapidly, and the estimator κ_t^{fluc} is error prone. To ensure that the update rule of Eq. (2) is reasonable at all times, we impose carefully defined lower and upper bounds for our final compressibility estimator,

$$\overline{\kappa}_t = \max\left[\kappa_t^{\min}, \min\left(\kappa_t^{\max}, \kappa_t^{\mathrm{fluc}}\right)\right]. \tag{6}$$

This ordering of the max and min operators ensures that $\overline{\kappa}_t$ never vanishes.

Imposing the *lower* bound $\kappa_t^{\min}$ protects against the case where early-time fluctuations of N are artificially small. This could happen in a QMC simulation, for example, if the initial guess $\mu_{t=0}$ is in one of the system's band gaps (N_t associated with fully occupied bands), leading to a divergence in $1/\kappa_t^{\mathrm{fluc}}$. Since the error in statistical observables decays like the inverse square root

of the number of samples, a reasonable lower bound on $\overline{\kappa}_t$ is given by

$$\kappa_t^{\min} = \frac{\alpha}{\sqrt{t+1}}, \tag{7}$$

for some appropriately defined α. Referring to Eq. (1), we see that κ should scale like the system volume V divided by an intensive energy. For the benchmarks in Sec. (III), we will select $\alpha = N_{\text{sites}}/u_0$ where N_{sites} is the number of lattice sites, and u_0 is a characteristic energy scale. Our tests indicate that algorithm performance is largely insensitive to the precise choice of α. By design, $\kappa_t^{\min}$ decays to zero at large times t.

Imposing the *upper* bound $\kappa_t^{\max}$ protects against the case where early-time fluctuations of N are artificially large. Although Eq. (5) is correct in thermodynamic equilibrium, it produces a very poor estimator in the *out-of-equilibrium* context of a dynamically evolving μ_t. Changes to μ_t will, by design, generate a strong response in N_t. Drift in N_t will cause a large overestimate of the compressibility, $\kappa_t^{\text{fluc}} \sim \overline{\text{Var}}_t[N] \sim V^2$. Recall that physical compressibility must scale like system size, $\kappa \sim V$, which is apparent from the definition $\kappa = \mathrm{d}\langle N\rangle/\mathrm{d}\mu$. To get a compressibility estimator with the correct scaling, we can compare the typical variations in N_t and μ_t. Specifically, we define the upper bound on $\overline{\kappa}_t$ to be

$$\kappa_t^{\max} = \sqrt{\frac{\overline{\text{Var}}_t[N]}{\overline{\text{Var}}_t[\mu]}}, \tag{8}$$

where $\overline{\text{Var}}_t[\mu]$ is the sample variance for $\{\mu_{t/2}, \ldots \mu_t\}$. At early times, when both μ_t and N_t are varying significantly, it is assured that $\kappa_t^{\max} \sim \overline{\kappa}_t \sim V$. At late times, μ_t should settle to the target chemical potential, whereas N_t will continue to exhibit equilibrium fluctuations. Then $\kappa_t^{\max}$ grows very large, and we expect to recover the fluctuation-based estimator, $\overline{\kappa}_t = \kappa_t^{\text{fluc}}$.

2. *Method summary*

Pseudocode for the full μ-tuning algorithm is listed in Algorithm 1. The mean and variance estimators can be updated in constant time using the methods described in Appendix A. The user must provide an initial guess $\mu_{t=0}$ for the chemical potential. Also required is a parameter α that sets an approximate scale for the compressibility.

We make two final remarks regarding the algorithm. Note, first, that convergence, $\overline{\mu}_{t+1} = \overline{\mu}_t$, implies that the target condition is satisfied, $\overline{N}_t = N^*$. Second, the dynamical update rules are inherently self-stabilizing. Suppose that changes to μ_t are having no major effect on N_t. Then the sample variance $\overline{\text{Var}}_t[N]$ will decrease, leading to smaller $\overline{\kappa}_t$. This, in turn, will drive larger updates to the chemical potential. Eventually the magnitude of these updates will be enough to produce the necessary changes in N_t. Conversely, if changes to μ_t are having too large of an effect on N_t, then compressibility estimator $\overline{\kappa}_t$ will also grow large, and this will dampen the magnitude of updates to μ_{t+1}. These self-stabilizing mechanisms share conceptual similarities to those in standard PID controllers [18, 19], though all parameters in our algorithm are physically motivated and work robustly across a range of systems.

Input: Target particle number N^*
Input: Initial guess $\mu_{t=0}$ for the chemical potential
Input: Characteristic compressibility scale α
for $t = 0, 1, \ldots$ **do**
  Perform MC sampling with chemical potential μ_t
  Collect samples for $\langle N\rangle$ and (in the QMC context) for $\langle N^2\rangle$
  Update time averages $\overline{\mu}_t$ and $\overline{N}_t$
  Update variance estimators $\overline{\text{Var}}_t[\mu]$ and $\overline{\text{Var}}_t[N]$
  Calculate κ estimate $\kappa_t^{\text{fluc}} = \beta\overline{\text{Var}}_t[N]$
  Calculate lower bound $\kappa_t^{\min} = \alpha/(t+1)^{1/2}$
  Calculate upper bound $\kappa_t^{\max} = \sqrt{\overline{\text{Var}}_t[N]/\overline{\text{Var}}_t[\mu]}$
  Calculate bounded κ estimate $\overline{\kappa}_t = \max(\kappa_t^{\min}, \min(\kappa_t^{\max}, \kappa_t^{\text{fluc}}))$
  Update $\mu_{t+1} = \bar{\mu}_t + (N^* - \overline{N}_t)/\overline{\kappa}_t$
end

Algorithm 1: Chemical potential tuning. In the language of magnetism, we would make the substitutions of Eq. (10).

III. RESULTS

A. Ising Model

We begin by demonstrating our method on a well-understood test case, the ferromagnetic Ising model on a two-dimensional square lattice. The Hamiltonian is

$$H = -J\sum_{\langle ij\rangle} s_i s_j - B\sum_i s_i, \tag{9}$$

where the sum over $\langle ij\rangle$ is over all nearest neighbor sites, and $s_i = \pm 1$. For simplicity, all energies will be measured in units of $J = 1$ and we likewise set the Boltzmann constant $k_{\text{B}} = 1$. The tunable quantity here is the magnetic field B, which couples linearly to the total magnetization $M = \sum_i s_i$. In this case, the magnetic susceptibility $\chi = \mathrm{d}\langle M\rangle/\mathrm{d}B = \beta\left(\langle M^2\rangle - \langle M\rangle^2\right)$ plays the role of the compressibility κ. Algorithm (1) applies upon making the following substitutions

$$\mu \mapsto B, \quad N \mapsto M, \quad \kappa \mapsto \chi. \tag{10}$$

It will also be convenient to refer to the magnetization per site, $m = M/N_{\text{sites}}$.

In zero field, this system undergoes a second-order phase transition between the paramagnetic and ferromagnetic phases at a critical temperature $T_c \approx 2.27$ [20]. Approaching T_c from above causes both the susceptibility χ and the autocorrelation time to diverge. The distance

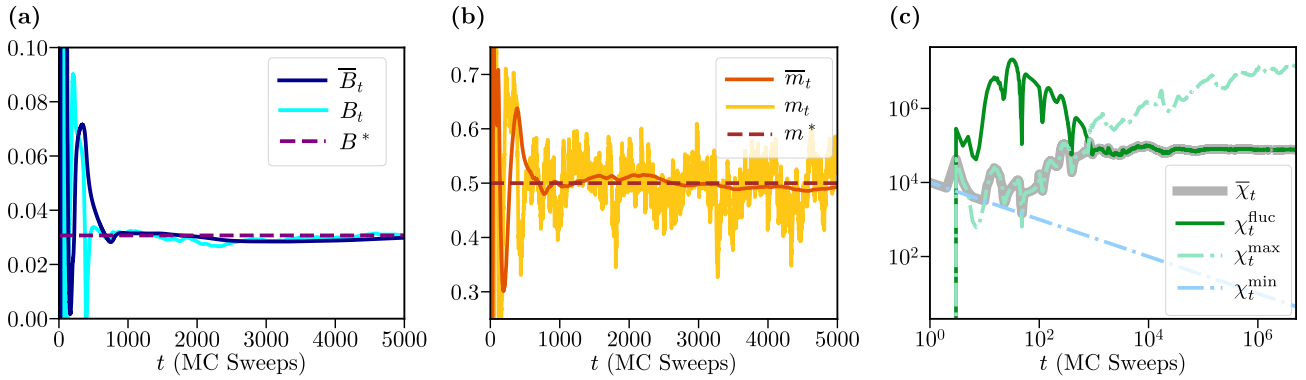

Figure 1: Tuning the magnetic field B of the classical Ising model to achieve a target magnetization per site, $m^* = 1/2$. We employ a 100×100 square lattice, and temperature $T = 2.5$. (a) The dynamically evolving field B_t and its running average $\overline{B}_t$ both eventually converge to $B^* \approx 3.096(2) \times 10^{-2}$. (b) Similar plots for $m_t = M_t/N_{\rm sites}$ and its running average $\overline{m}_t$; significant equilibrium fluctuations in m_t are observed. (c) The susceptibility χ (analogous to κ) is reasonably estimated by $\overline{\chi}_t$, with the lower and upper bounds, $\chi_t^{\rm min}$ and $\chi_t^{\rm max}$, playing important roles at early times. At long times the susceptibility converges to $7.76(4) \times 10^4$. Note that panel (c) is a log-log plot and extends over longer times than panels (a) and (b).

$T - T_c$ from the critical point offers an excellent means to scale the "tuning difficulty".

To begin, we investigate an example tuning run on a 100×100 Ising system at a temperature of $T = 2.5$, starting with a uniformly random initial state. By symmetry, zero magnetization is achieved at zero field. To make the tuning task more interesting, we aim to find the magnetic field $B = B^*$ that produces a *nonzero* target magnetization-per-site of $m^* = 1/2$. Despite the presence of a small but finite field $B^* > 0$, we still observe very large autocorrelation times when T approaches T_c. To explore this effective critical slowing down, we opt to use the standard single spin-flip Metropolis-Hastings algorithm [21], though more advanced cluster updates [22, 23] would also be compatible with the tuning algorithm. The time index t is incremented once per MC sweep, at which point a new measurement of the total magnetization M_t is taken, and the field B_{t+1} is computed according to Algorithm 1 under the substitutions of Eq. (10). The initial field is $B_{t=0} = 0$. To set a scale for $\chi_t^{\rm min}$, we select $\alpha = N_{\rm sites}/J$.

In Fig. 1, we plot the result of dynamically tuning the field B_t. Panels 1(a) and 1(b) show the time evolution of B_t and m_t, and their time averages. Panel 1(c) shows estimators for the susceptibility χ (compressibility κ in lattice gas language). The dynamics undergoes three different regimes, corresponding to the three branches in the expression $\overline{\chi}_t = \max\left[\chi_t^{\rm min}, \min\left(\chi_t^{\rm max}, \chi_t^{\rm fluc}\right)\right]$. For the first few MC sweeps ($t \leq 3$) there is essentially no good susceptibility data. Here, the lower bound $\chi_t^{\rm min}$ of Eq. (7) controls the estimator $\overline{\chi}_t$ and prevents the algorithm from making overly large corrections to B_t. In the intermediate time regime of $3 < t \lesssim 10^3$, the field B_t is evolving significantly, and driving large changes to m_t. Here, the upper bound $\chi_t^{\rm max}$ of Eq. (8) controls the estimator $\overline{\chi}_t$ and correctly captures the approximate sensitivity of magnetism to changes in the applied field. By the end of this regime, fluctuations in B_t decrease significantly. Finally, at times $t \gtrsim 10^3$, the fluctuation-based estimator $\chi_t^{\rm fluc}$ becomes accurate, and B_t converges precisely toward the solution $B^* \approx 3.096 \times 10^{-2}$.

In Fig. 2, we show the evolution of B_t for the same Ising model, but now over a variety of temperatures. At high T, the tuner converges to the correct value B^* very quickly. At temperatures approaching $T_c \approx 2.27$, both the autocorrelation time and the magnetic susceptibil-

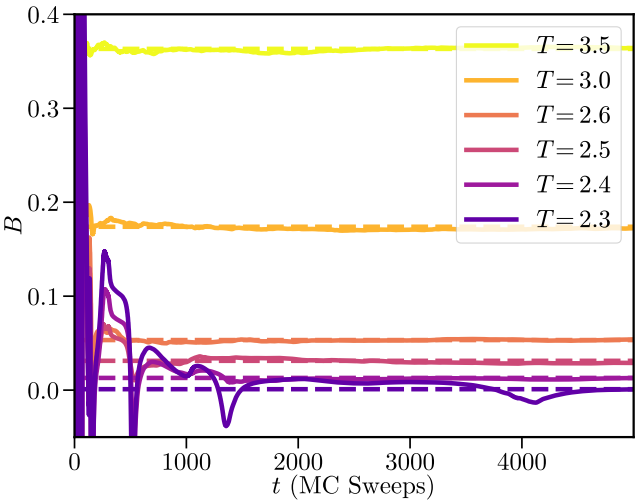

Figure 2: Dynamically tuning the magnetic field B_t (solid lines) towards the solution B^* (dashed lines) which achieves a target magnetization per site $m^* = 1/2$ for various temperatures above $T_c \approx 2.27$. The most challenging case tested is $T = 2.3$, for which early-time values of B_t can go as high as 2.

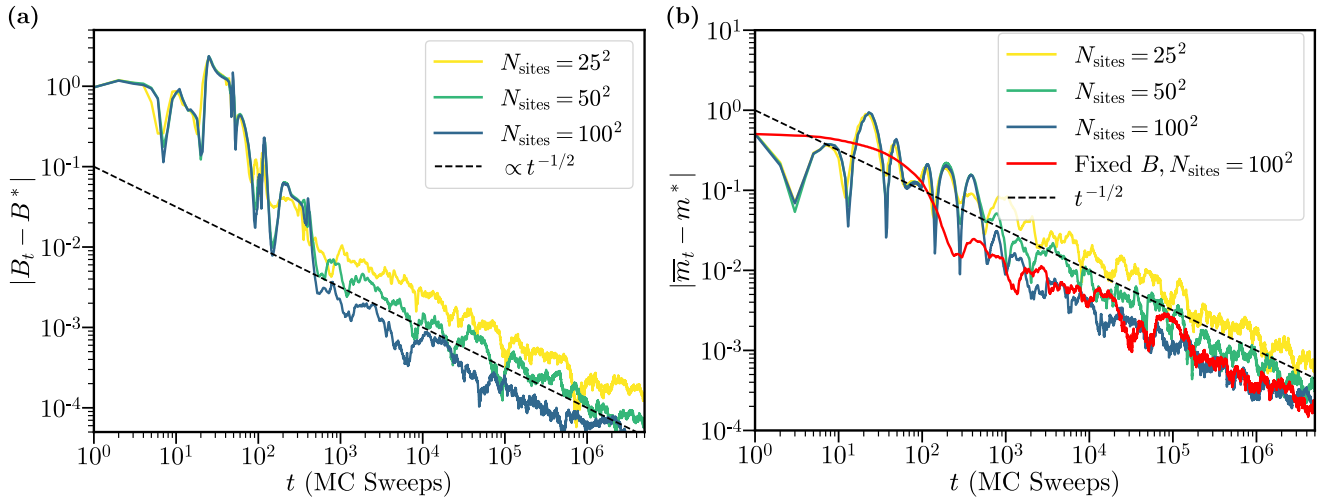

Figure 3: Errors in (a) the dynamically-tuned magnetic field and (b) the running-mean magnetization. We consider Ising systems of various sizes, with $T = 2.5$ and target magnetization $m^* = 0.5$. Error curves are averaged over 10 independent runs. The reference magnetizations B^* are estimated, per system size, by averaging B_t at $t = 5 \times 10^6$ over all 10 runs. The red curve in (b) results from a $N_{\text{sites}} = 100^2$ simulation where $B = B^*$ is held fixed throughout the entire simulation.

ity grow large, leading to difficulty in collecting accurate statistics, and very high sensitivity to small changes in the applied field. Despite the slower convergence near T_c, the tuner appears to be working correctly in all cases tested.

Figure 3 shows the error of the instantaneous field $|B_t - B^*|$ and the running-mean magnetization $|\bar{m}_t - m^*|$, throughout the tuning process. Here we take $T = 2.5$ and $m^* = 1/2$ as in Fig. 1, and allow system size to vary. Our best estimates for B^* are obtained by averaging over 10 independent runs, extending to $t = 5 \times 10^6$ Monte Carlo sweeps. The results are $B^* = 3.113(3) \times 10^{-2}$ and $B^* = 3.096(1) \times 10^{-2}$, for lattice sizes $N_{\text{sites}} = 25^2$ and 100^2, respectively. The system size dependence is relatively minor, given our choice of $T = 2.5$. At temperatures nearer to $T_c \approx 2.27$, the B^* would become smaller, and their relative variation would depend more strongly on system size.

The early time dynamics (up to $\sim 10^2$ sweeps) of both errors are seen to be system-size independent due to the dynamics being dominantly controlled by our χ^{min} and χ^{max} bounding scheme. Once χ^{fluc} gains control, we can see a separation emerge as larger systems enjoy improved statistics from increased self-averaging, resulting in faster tuning. At these large times, the errors decay as $t^{-1/2}$, and the limiting factor in tuning becomes the statistical error in the Monte Carlo estimates. In this regime, note that the error in the average magnetization, $|\bar{m}_t - m^*|$, is roughly independent of whether B_t is being tuned dynamically, or fixed to the correct value $B = B^*$ throughout the simulation [shown as the red curve in Fig. 3(b)].

B. Holstein Model

We now demonstrate our method in a quantum Monte Carlo (QMC) setting. As a test case we consider the Holstein model, one of the simplest models describing interactions between electrons and phonons on a lattice [24]. The Hamiltonian is

$$\hat{H} = -t_{\text{h}} \sum_{\langle \boldsymbol{ij} \rangle, \sigma} (\hat{c}^\dagger_{\boldsymbol{i},\sigma} \hat{c}_{\boldsymbol{j},\sigma} + \text{h.c.}) - \mu \sum_{\boldsymbol{i},\sigma} \hat{n}_{\boldsymbol{i},\sigma} + \frac{1}{2} \sum_{\boldsymbol{i}} \hat{P}^2_{\boldsymbol{i}} + \frac{\omega^2}{2} \sum_{\boldsymbol{i}} \hat{X}^2_{\boldsymbol{i}} + \lambda \sum_{\boldsymbol{i},\sigma} \hat{n}_{\boldsymbol{i},\sigma} \hat{X}_{\boldsymbol{i}}. \quad (11)$$

The operator $\hat{c}^\dagger_{\boldsymbol{i},\sigma}$ creates an electron on site $\boldsymbol{i}$ with spin σ, and $\hat{n}_{\boldsymbol{i},\sigma} = \hat{c}^\dagger_{\boldsymbol{i},\sigma} \hat{c}_{\boldsymbol{i},\sigma}$ is the electron number. The first term in $\hat{H}$ describes hopping between nearest-neighbor sites $\langle \boldsymbol{ij} \rangle$. The Hamiltonian also includes bosonic position and momentum operators, $\hat{X}_{\boldsymbol{i}}$ and $\hat{P}_{\boldsymbol{i}}$, which models a local phonon mode on site $\boldsymbol{i}$ with frequency ω. The term proportional to λ couples the electrons and phonons leading to a phonon mediated effective electron-electron interaction. We set our energy units in terms of the hopping amplitude $t_{\text{h}} = 1$, in which the value of the chemical potential needed to obtain half-filling (i.e. one electron/site on average) is known to be $\mu = -\frac{\lambda^2}{\omega^2}$ from a particle-hole transformation [25]. Due to the Pauli exclusion principle, at most two electrons can exist on a single site.

The total electron number operator is $\hat{N} = \sum_{\boldsymbol{i},\sigma} \hat{n}_{\boldsymbol{i},\sigma}$. Our goal is to tune the chemical potential μ to produce a target density, $\langle \hat{N} \rangle = N^*$. Here, the expectation of an

observable $\hat{\mathcal{O}}$ is understood to mean

$$\left\langle \hat{\mathcal{O}} \right\rangle = \mathcal{Z}^{-1} \mathrm{Tr}\, e^{-\beta \hat{H}} \hat{\mathcal{O}}, \tag{12}$$

$$\mathcal{Z} = \mathrm{Tr}\, e^{-\beta \hat{H}}, \tag{13}$$

and the trace runs over the entire Fock space.

1. Overview of quantum Monte Carlo

There are many forms of QMC. One widely used set of methods begins by expressing the many-body partition function $Z = \mathrm{Tr}\, e^{-\beta \hat{H}}$ as a path integral involving fields that fluctuate in imaginary time. The aim is then to perform *ordinary* Monte Carlo sampling of these fluctuating variables according to some appropriate probability distribution. In the determinant-QMC approach [6], which is our focus here, one uses a Suzuki-Trotter expansion inside the trace

$$Z = \mathrm{Tr} \underbrace{e^{-\Delta\tau \hat{H}_0} e^{-\Delta\tau \hat{H}_1} \cdots e^{-\Delta\tau \hat{H}_0} e^{-\Delta\tau \hat{H}_1}}_{\beta/\Delta t \text{ imaginary time slices}} + \mathcal{O}(\Delta\tau^2), \tag{14}$$

with a carefully selected decomposition $\hat{H} = \hat{H}_0 + \hat{H}_1$. Inserting a complete set of states at each discrete imaginary time slice, $0 \le \tau < \beta$, introduces an effectively classical field $x_{\tau,\boldsymbol{i}}$ which, when sampled, allows to estimate observables $\left\langle \hat{\mathcal{O}} \right\rangle$. Each sample $x_{\tau,\boldsymbol{i}}$ is typically weighted according to a fermionic determinant, $P[x] \propto \left| \det M_\uparrow^\dagger M_\downarrow \right|$, for an appropriate matrix function $M_\sigma[x]$.

When this procedure is applied to the Holstein model, the field $x_{\tau,\boldsymbol{i}}$ can be interpreted as "imaginary time fluctuations" of the phonons. An analogous formalism is used for sampling the gluon field in lattice quantum chromodynamics (QCD), and we can borrow techniques from that community. In particular, Langevin [7] and hybrid Monte Carlo (HMC) sampling [26, 27] have both proven effective for simulating electron-phonon models [28, 29], and make it possible to update the entire field $x_{\tau,\boldsymbol{i}}$ at a cost that scales near-linearly with system size. Here we employ HMC. A complete account of our QMC methodology is presented in [30].

2. Chemical potential tuning for quantum models

Algorithm 1 remains valid in the QMC context provided that we are careful in estimating the compressibility κ. The thermodynamic relationship of Eq. (1) continues to hold,

$$\kappa = \frac{\mathrm{d}\langle \hat{N} \rangle}{\mathrm{d}\mu} = \beta \mathrm{Var}[\hat{N}], \tag{15}$$

where $\mathrm{Var}[\hat{N}] = \langle \hat{N}^2 \rangle - \langle \hat{N} \rangle^2$, and each expectation value on the right-hand side is to be interpreted in the sense of Eq. (12). An interesting feature of QMC, however, is that unbiased samples N_t of $\langle \hat{N} \rangle$ do *not* generally contain sufficient information to estimate the variance of $\hat{N}$ due to neglecting within-sample fluctuations [31]. We can still define a fluctuation-based estimator in the form of Eq. (5),

$$\kappa_t^{\mathrm{fluc}} = \beta \overline{\mathrm{Var}}_t[\hat{N}], \tag{16}$$

but now we must use

$$\overline{\mathrm{Var}}_t[\hat{N}] = \overline{N_t^{(2)}} - \left(\overline{N}_t\right)^2, \tag{17}$$

where $N_t^{(2)}$ denotes a statistical sample of the expectation value $\langle \hat{N}^2 \rangle$ defined in Eq. (12). Time-averages have the same form as in Eqs. (3) and (4), but now we must also track,

$$\overline{N_t^{(2)}} = \frac{1}{L_t} \sum_{t'=\lceil t/2 \rceil}^{t} N_{t'}^{(2)}. \tag{18}$$

The quantity $\kappa_t^{\max}$ remains as in Eq. (8), but using the sample variance of Eq. (17). With these refinements to κ_t^{fluc} and $\kappa_t^{\max}$, we can directly apply Algorithm 1 to tune the chemical potential.

3. Single-Site Limit

As an initial demonstration, we examine the behavior of Algorithm 1 in the single-site limit of the Holstein model ($t_h = 0$). This model admits an analytic solution by the Lang-Firsov transformation [32, 33], but nonetheless serves as a challenging test-case for μ-tuning. The effective action $S[x]$ resulting from Eq. (11) possesses two deep local minima (associated with electron number 0 or 2) due to an effective electron-electron attraction that is mediated by the phonons. MC sampling of the phonon field x_τ is characterized by long periods of trapping within one minima, punctuated by rare hops across the barrier into the other. Strong hysteresis creates a challenge for μ-tuning; adjusting the chemical potential μ_t may affect measurements of electron number $N_{t'}$ only after a very large amount of simulation time, $t' \gg t$.

We consider a model with $\omega = 1, \lambda = \sqrt{2}$ at $\beta = 4$. These are values commonly used in studies of the charge density wave transition in the Holstein model, which occurs at $\beta_c \sim 6$ when $t_h = 1$ [34]. We aim for a target electron number of $\langle \hat{N} \rangle = 1$, i.e. half filling. This corresponds to finding the chemical potential at which the average occupancies of the two metastable states are equal. In the single site limit at half filling, the exact chemical potential and compressibility are $\mu^* = -\lambda^2/\omega^2$ and $\kappa^* = \beta/(1 + e^{\beta\mu^*/2})$. We use an initial guess for the chemical potential, $\mu_0 = 0$, that is purposefully distant from the true value $\mu^* = -2$. To set a scale for $\kappa_t^{\min}$, we select $\alpha = N_{\mathrm{sites}}/\omega$.

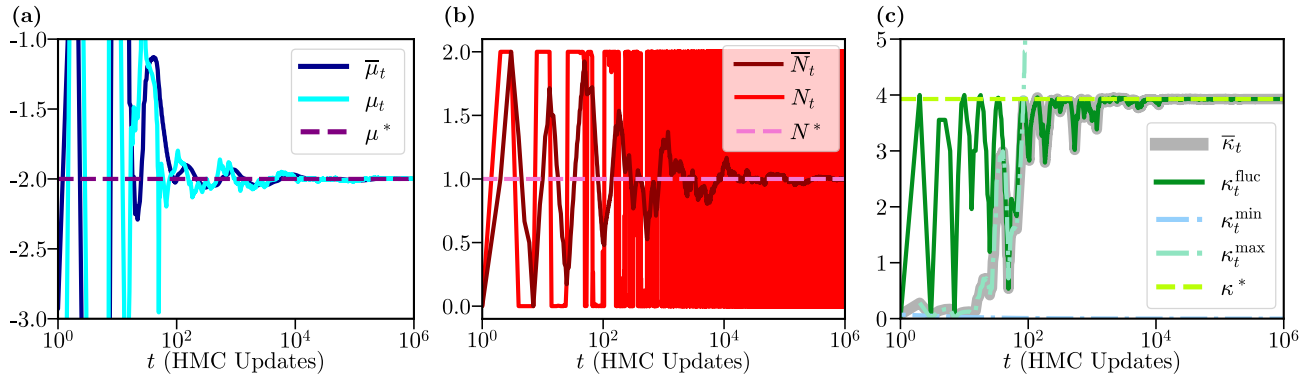

Figure 4: Tuning the chemical potential μ_t of a single-site Holstein model with $\omega = 1$, $\lambda = \sqrt{2}$, and $\beta = 4$ to achieve half-filling, $N^* = 1$. The target chemical potential is exactly $\mu^* = -2$. Early time fluctuations in μ_t are of order 10. In the absence of dynamical μ-tuning, the natural transition rate between metastable wells is of order $\Delta t = 10^2$.

Figure 4 illustrates a representative μ-tuning run. Each increment in time t corresponds to a single HMC trial update. At early times, Fig. 4(b) shows sharp transitions ("jumps") in the measurements N_t, which are largely driven by changes in μ_t. These jumps correspond to transitions between the two metastable wells, and in the absence of μ-tuning, would occur on the time-scale of 10^2 HMC trial updates.

Figure 4(c) shows that each of the early-time jumps between metastable wells is accompanied by a large spike in $\bar{\kappa}_t$, which reflects the large change in N_t. After each jump, there is a significant period of time where N_t is roughly constant, which causes $\bar{\kappa}_t$ to drop. At times $t \lesssim 100$, the upper bound $\kappa^{\max}$ is instrumental in allowing the tuning dynamics to make significant corrections to μ, which drive the density back and forth between metastable wells on an exponentially growing time scale. At around $t \approx 100$, we reach the time scale required for natural (equilibrium) jumps between the the two metastable wells. At this point, the algorithm switches over to the fluctuation-based compressibility estimator $\bar{\kappa}_t = \kappa_t^{\rm fluc}$, as observed Fig. 4(c). At times $t \gtrsim 100$, the errors in statistical estimators decay like $t^{-1/2}$ in a controlled fashion.

4. *Full 2D system*

Finally, to benchmark our algorithm in a more realistic setting, we consider a square lattice Holstein model with phonon frequency $\omega = 1$ and coupling strength $\lambda = \sqrt{2}$. We consider a square lattice of size $L = 10$, with $N_{\rm sites} = L^2$ total sites. At half-filling the ground state is characterized by a finite temperature phase transition to charge-density-wave (CDW) order, where the electrons localize onto one of the two sublattices, spontaneously breaking a $\mathbb{Z}_2$ symmetry. For our chosen parameters the critical inverse temperature is approximately $\beta \sim 6$.

We test our algorithm at an inverse temperature $\beta = 10$. At half-filling, this low temperature gives rise to a gapped CDW phase. When doped sufficiently away from half filling, and at sufficiently low temperature, the system is expected to transition to a superconducting phase[35, 36].

We measure the CDW order using the staggered charge susceptibility

$$\chi_{\rm cdw} = \int_0^\beta \sum_{\boldsymbol{r}} (-1)^{(r_x + r_y)} C(\boldsymbol{r}, \tau)\, d\tau, \tag{19}$$

defined in terms of the real-space density-density correlation function

$$C(\boldsymbol{r}, \tau) = \frac{1}{N} \sum_{\boldsymbol{i}} \langle \hat{n}_{\boldsymbol{i}+\boldsymbol{r}}(\tau) \hat{n}_{\boldsymbol{i}}(0) \rangle\,, \tag{20}$$

where $\hat{n}_{\boldsymbol{i}}(\tau) = \hat{n}_{\boldsymbol{i},\downarrow}(\tau) + \hat{n}_{\boldsymbol{i},\uparrow}(\tau)$ denotes the total electron number on site $\boldsymbol{i}$ at imaginary time τ. A signature for superconducting order is given by the pair susceptibility

$$P_s = \frac{1}{N_{\rm sites}} \int_0^\beta \left\langle \hat{\Delta}(\tau)\, \hat{\Delta}^\dagger(0) \right\rangle d\tau, \tag{21}$$

where $\hat{\Delta}(\tau) = \sum_i \hat{c}_{\boldsymbol{i},\downarrow}(\tau)\, \hat{c}_{\boldsymbol{i},\uparrow}(\tau)$.

In Fig. 5 we compare two sets of simulation results, one where μ is held fixed, and the other where we tune μ to a target density that was measured in the first set of results. All simulations employed $t = 5 \times 10^3$ thermalization HMC steps. Following this, we performed 5×10^4 steps, with measurements taken at every step. For the dynamical μ simulations we initialized the chemical potential to $\mu_{t=0} = 0$ and set $\alpha = N_{\rm sites}/\omega$. The chemical potential was continually updated throughout the simulation, but had largely converged already by the end of the thermalization process. There is very good agreement between the two sets of data; the error bars with μ-tuning enabled are not discernibly larger than with μ fixed to its target value.

Figure 5(a) shows the density as a function of the chemical potential. The plateau at half filling ($\mu = -2$) illustrates the gapped CDW phase. The relatively large

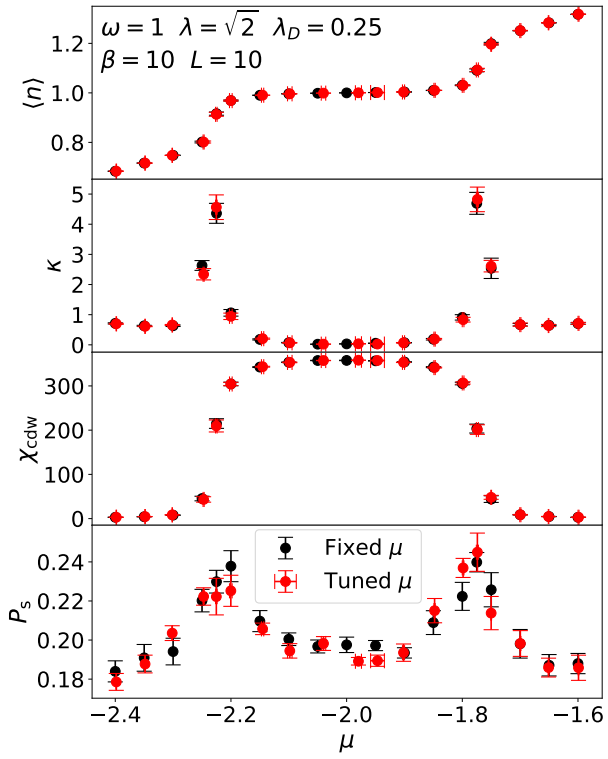

Figure 5: Comparison of several observables measured in a 10×10 Holstein model under the fixed-μ scheme (black), and under dynamic μ-tuning scheme aiming to achieve a target density (red). Horizontal error bars on the red markers indicate uncertainty as measured by the standard error of μ.

horizontal error bars in the tuned value of μ near half-filling are associated with a vanishing compressibility κ, Fig. 5(b). In other words, a fairly wide range of chemical potentials give rise to (approximately) half-filling. Observe that the plateau in $\langle n \rangle = \langle N \rangle / N_{\mathrm{sites}}$ corresponds to a strong enhancement of χ_{cdw} in Fig. 5(c) and a suppression of P_s in Fig. 5(d). With enough doping, at approximately $\mu = -2.3$ and $\mu = -1.7$, the marker χ_{cdw} for CDW order rapidly vanishes. Simultaneously, the density rapidly shifts away from half-filling, as reflected by the two peaks in the compressibility κ. We emphasize that the μ-tuning algorithm performs well throughout the diverse range of behaviors exhibited in this model.

IV. DISCUSSION

The dynamical μ-tuning algorithm presented in Algorithm 1 enables simulation in the grand-canonical ensemble while targeting a fixed mean particle number. The algorithm is straightforward to implement, and imposes negligible computational overhead. Note that all running time averages can be updated in constant time using the formulas of Appendix A.

Under the proposed scheme, the chemical potential μ is adjusted concurrently with the MC sampling. Although we do not provide formal convergence guarantees, the method works well in practice. For long-running simulations, most statistical samples will be collected after μ has approximately converged to its target value, and our benchmarks show that errors are well controlled.

Models with long autocorrelation times present a practical challenge, in that it becomes difficult to assess the impact of a modified μ value on the resulting mean particle number $\langle N \rangle$. Our solution is to effectively collect statistics over increasingly large time-windows such that, eventually, both $\langle N \rangle$ and its sensitivity $\kappa = \mathrm{d}\langle N \rangle / \mathrm{d}\mu$ can be accurately measured. We demonstrated that our scheme works well even in very challenging cases, such as the Ising model approaching criticality, and the single-site Holstein model with strong metastability due to phonon-mediated electron binding and associated large energy barriers. The method also works well for larger-size quantum Monte Carlo simulations of the Holstein model on the square lattice, including at filling fractions coinciding with a charge density wave gap, where κ approximately vanishes.

Many variations of the μ-tuning algorithm could be studied. For example, one could modify the definition of the running time averages in Eqs. (3) and (4) to "smoothly forget" past data, with the goal of reducing underdamped oscillations in the early-time dynamics of the tuned field, e.g., in Figs. 1(a) and 4(a). One might also explore whether ideas for accelerating fixed point solvers (e.g., Anderson mixing) could somehow be incorporated into Eq. (2), which updates μ as a correction to the time-average $\overline{\mu}$. In our preliminary tests, however, we could not find any modifications to the algorithm that significantly improved accuracy over large simulation times. Indeed, Figs. 3 and 5 suggest that the μ-tuning algorithm is already close to optimal; errors in long-time statistical measurements are observed to be about the same, whether μ is dynamically tuned or statically fixed to the exactly correct value.

ACKNOWLEDGMENTS

K. B. acknowledges support from the Center of Materials Theory as a part of the Computational Materials Science (CMS) program, funded by the U.S. Department of Energy, Office of Basic Energy Sciences. S. J., O. B., and R. T. S. acknowledge support from the U.S. Department of Energy, Office of Science, Office of Basic Energy Sciences, under Award Number DE-SC0022311. C. M. acknowledges support by the U.S. Department of Energy, Office of Science, Office of Advanced Scientific Computing Research, Department of Energy Computational Graduate Fellowship under Award Number DE-SC0020347. B. C.-S. was funded by a U.C. National Laboratory In-Residence Graduate Fellowship through the U.C. National Laboratory Fees Research Program.

AUTHOR DECLARATIONS

The authors have no conflicts to disclose.

CODE AVAILABILITY

Code and an interactive interface to explore tuning for the Ising system is available at https://colemiles.github.io/ising-tuner. Code for Holstein simulations, with μ-tuning built-in, is available at https://github.com/cohensbw/ElPhDynamics.

Appendix A: Updating running time-averages

The μ-tuning algorithm require to maintain running averages of the form

$$\overline{x}_t = \frac{1}{L_t} \sum_{t'=\lceil ct \rceil}^{t} x_{t'}, \tag{A1}$$

where $L_t = t - \lceil ct \rceil + 1$ is the count of samples in the average, and $\lceil \cdot \rceil$ denotes the ceiling function. We selected $c = 1/2$ for our study, but other values $0 < c < 1$ are possible. The x_t data could be one of the following: the instantaneous chemical potential μ_t, a sample N_t for the particle number, or (in the QMC context) a sample $N_t^{(2)}$ for the particle number squared.

After each MC time step, we wish to update the running average from $\overline{x}_t$ to $\overline{x}_{t+1}$. It is helpful to distinguish between two cases,

$$\begin{aligned} \text{Case A}: &\ \lceil c(t+1) \rceil = \lceil ct \rceil \\ \text{Case B}: &\ \lceil c(t+1) \rceil = \lceil ct \rceil + 1. \end{aligned}$$

These are the only two possibilities given our assumptions that $0 < c < 1$ and t is integer.

In Case A we must add the new datapoint x_{t+1} to the running average. In Case B we must additionally remove the datapoint $x_{\lceil ct \rceil}$ from the running average. The update rule is then,

$$\overline{x}_{t+1} = \begin{cases} (L_t \overline{x}_t + x_{t+1})/L_{t+1} & \text{Case A} \\ (L_t \overline{x}_t + x_{t+1} - x_{\lceil ct \rceil})/L_{t+1} & \text{Case B.} \end{cases} \tag{A2}$$

In Case A the number of datapoints increases by one, $L_{t+1} = L_t + 1$, whereas in Case B, $L_{t+1} = L_t$. We can therefore rearrange as,

$$\overline{x}_{t+1} = \begin{cases} \overline{x}_t + (x_{t+1} - \overline{x}_t)/L_{t+1} & \text{Case A} \\ \overline{x}_t + (x_{t+1} - x_{\lceil ct \rceil})/L_{t+1} & \text{Case B,} \end{cases} \tag{A3}$$

which improves numerical accuracy.

We are also interested in keeping a running estimate of the sample variance,

$$\overline{\text{Var}}_t[x] = \overline{x_t^2} - (\overline{x}_t)^2, \tag{A4}$$

or, for quantum observables, the closely related Eq. (17). The formula suggests that we maintain a running average $\overline{x_t^2}$, through which the variance follows immediately. To estimate $\text{Var}[\hat{N}]$ in QMC simulations, such a strategy may be necessary. Whenever possible, however, direct numerical implementation of Eq. (A4) should be avoided due to potentially large floating point round-off error. A much improved algorithm was proposed by Welford [37], which we here adapt.

The sample variance can be equivalently written,

$$\overline{\text{Var}}_t[x] = M_t / L_t, \tag{A5}$$

where

$$M_t = \sum_{t'=\lceil ct \rceil}^{t} (x_{t'} - \overline{x}_t)^2. \tag{A6}$$

After a somewhat lengthy derivation, one finds the recursion relation,

$$M_{t+1} = \begin{cases} M_t + (x_{t+1} - \overline{x}_t)(x_{t+1} - \overline{x}_{t+1}) & \text{Case A} \\ M_t + \left(x_{t+1} - x_{\lceil ct \rceil}\right)\left(x_{t+1} - \overline{x}_{t+1} + x_{\lceil ct \rceil} - \overline{x}_t\right) & \text{Case B,} \end{cases} \tag{A7}$$

which is numerically stable and easy to implement given that we are already maintaining the running average $\overline{x}_t$. Note that Cases A and B coincide when $x_{\lceil ct \rceil} = \overline{x}_t$.

[1] J. Yao, R. A. Greenkorn, and K. C. Chao, Monte Carlo simulation of the grand canonical ensemble, Mol. Phys. **46**, 587 (1982).

[2] F. A. Escobedo and J. J. de Pablo, Expanded grand canonical and Gibbs ensemble Monte Carlo simulation of polymers, J. Chem. Phys. **105**, 4391 (1996).

[3] P. Kowalczyk, H. Tanaka, R. Hołyst, K. Kaneko, T. Ohmori, and J. Miyamoto, Storage of Hydrogen at 303 K in Graphite Slitlike Pores from Grand Canonical Monte Carlo Simulation, J. Phys. Chem. B **109**, 17174 (2005).

[4] M. Clark, F. Guarnieri, I. Shkurko, and J. Wiseman, Grand Canonical Monte Carlo Simulation of Ligand-Protein Binding, J. Chem. Inf. Model. **46**, 231 (2006).

[5] H. Eslami and F. Müller-Plathe, Molecular dynamics simulation in the grand canonical ensemble, J. Comp. Chem. **28**, 1763 (2007).

[6] R. Blankenbecler, D. J. Scalapino, and R. L. Sugar, Monte Carlo calculations of coupled boson-fermion systems. I, Phys. Rev. D **24**, 2278 (1981).

[7] G. G. Batrouni, G. R. Katz, A. S. Kronfeld, G. P. Lepage, B. Svetitsky, and K. G. Wilson, Langevin simulations of lattice field theories, Phys. Rev. D **32**, 2736 (1985).

[8] R. T. Scalettar, D. J. Scalapino, R. L. Sugar, and D. Toussaint, Hybrid molecular-dynamics algorithm for the numerical simulation of many-electron systems, Phys. Rev. B **36**, 8632 (1987).

[9] S. R. White, D. J. Scalapino, R. L. Sugar, E. Y. Loh, J. E. Gubernatis, and R. T. Scalettar, Numerical study of the two-dimensional Hubbard model, Phys. Rev. B **40**, 506 (1989).

[10] N. Kawashima, J. E. Gubernatis, and H. G. Evertz, Loop algorithms for quantum simulations of fermion models on lattices, Phys. Rev. B **50**, 136 (1994).

[11] S. Zhang, Finite-temperature Monte Carlo calculations for systems with fermions, Phys. Rev. Lett. **83**, 2777 (1999).

[12] Y.-Y. He, M. Qin, H. Shi, Z.-Y. Lu, and S. Zhang, Finite-temperature auxiliary-field quantum Monte Carlo: Self-consistent constraint and systematic approach to low temperatures, Phys. Rev. B **99**, 045108 (2019).

[13] J. E. Hirsch, R. L. Sugar, D. J. Scalapino, and R. Blankenbecler, Monte Carlo simulations of one-dimensional fermion systems, Phys. Rev. B **26**, 5033 (1982).

[14] A. W. Sandvik, Finite-size scaling of the ground-state parameters of the two-dimensional Heisenberg model, Phys. Rev. B **56**, 11678 (1997).

[15] S. Zhang, J. Carlson, and J. E. Gubernatis, Constrained path quantum Monte Carlo method for fermion ground states, Phys. Rev. Lett. **74**, 3652 (1995).

[16] S. Zhang, J. Carlson, and J. E. Gubernatis, Constrained path Monte Carlo method for fermion ground states, Phys. Rev. B **55**, 7464 (1997).

[17] J. A. Speidel, J. R. Banfelder, and M. Mezei, Automatic Control of Solvent Density in Grand Canonical Ensemble Monte Carlo Simulations, J. Chem. Theory Comput. **2**, 1429 (2006).

[18] K. G. Kleiner, Implementing a Self-Corrected Chemical Potential Scheme in Determinant Quantum Monte Carlo Simulations, Chancellor's Honors Project (2019).

[19] J. Bechhoefer, Feedback for physicists: A tutorial essay on control, Rev. Mod. Phys. **77**, 783 (2005).

[20] L. Onsager, Crystal statistics. I. A two-dimensional model with an order-disorder transition, Phys. Rev. **65**, 117 (1944).

[21] W. K. Hastings, Monte Carlo sampling methods using Markov chains and their applications, Biometrika **57**, 97 (1970).

[22] J.-S. Wang and R. H. Swendsen, Cluster Monte Carlo algorithms, Physica A **167**, 565 (1990).

[23] J. Kent-Dobias and J. P. Sethna, Cluster representations and the Wolff algorithm in arbitrary external fields, Phys. Rev. E **98**, 063306 (2018).

[24] T. Holstein, Studies of polaron motion: Part i. the molecular-crystal model, Annals of physics **8**, 325 (1959).

[25] S. Johnston, E. A. Nowadnick, Y. F. Kung, B. Moritz, R. T. Scalettar, and T. P. Devereaux, Determinant quantum Monte Carlo study of the two-dimensional single-band Hubbard-Holstein model, Phys. Rev. B **87**, 235133 (2013).

[26] S. Duane, A. D. Kennedy, B. J. Pendleton, and D. Roweth, Hybrid Monte Carlo, Phys. Lett. B **195**, 216 (1987).

[27] R. Neal, MCMC Using Hamiltonian Dynamics, in *Handbook of Markov Chain Monte Carlo* (Chapman and Hall/CRC, 2011).

[28] G. G. Batrouni and R. T. Scalettar, Langevin simulations of a long-range electron-phonon model, Phys. Rev. B **99**, 035114 (2019).

[29] S. Beyl, F. Goth, and F. F. Assaad, Revisiting the hybrid quantum Monte Carlo method for Hubbard and electron-phonon models, Phys. Rev. B **97**, 085144 (2018).

[30] B. Cohen-Stead, O. Bradley, C. Miles, G. Batrouni, R. Scalettar, and K. Barros, Fast and scalable quantum Monte Carlo simulations of electron-phonon models, arXiv:2203.01291 (2022).

[31] Classical microstates sampled from the grand canonical equilibrium distribution have a well defined particle number. Our QMC simulations, in contrast, sample a phonon field that fluctuates in imaginary time, and each phonon configuration is associated with an entire statistical distribution of electron numbers.

[32] I. G. Lang and Y. A. Firsov, Zh. Éksp. Teor. Fiz. **43**, 1843 (1962), [Sov. Phys. JETP 16, 1301 (1963)].

[33] G. D. Mahan, *Many Particle Physics, Third Edition* (Plenum, New York, 2000).

[34] C. Feng and R. T. Scalettar, Interplay of flat electronic bands with Holstein phonons, Phys. Rev. B **102**, 235152 (2020).

[35] O. Bradley, G. G. Batrouni, and R. T. Scalettar, Superconductivity and charge density wave order in the two-dimensional Holstein model, Phys. Rev. B **103**, 235104 (2021).

[36] B. Nosarzewski, E. W. Huang, P. M. Dee, I. Esterlis, B. Moritz, S. A. Kivelson, S. Johnston, and T. P. Devereaux, Superconductivity, charge density waves, and bipolarons in the Holstein model, Phys. Rev. B **103**, 235156 (2021).

[37] B. P. Welford, Note on a Method for Calculating Corrected Sums of Squares and Products, Technometrics **4**, 419 (1962).